Engineering Science and Technology, an International Journal xxx (2014) 1–13

HOSTED BY

Contents lists available at ScienceDirect

Engineering Science and Technology, an International Journal

journal homepage: http://www.elsevier.com/locate/jestch

Full length article

CFD analysis for H-rotor Darrieus turbine as a low speed wind energy converter

M.H. Mohamed*, A.M. Ali, A.A. Hafiz

Mechanical Power Engineering Dept., Faculty of Engineering – Mattaria, Helwan University, P.O. 11718, Cairo, Egypt

ARTICLE INFO

Article history:
Received 11 May 2014
Received in revised form
4 August 2014
Accepted 6 August 2014
Available online xxx

Keywords:
Wind turbines
Meshing
Darrieus turbine
CFD
Turbulence models
Pitch angle

ABSTRACT

Vertical axis wind turbines like the Darrieus turbine appear to be promising for the conditions of low wind speed, but suffer from a low efficiency compared to horizontal axis turbines. A fully detailed numerical analysis is introduced in this work to improve the global performance of this wind turbine. A comparison between ANSYS Workbench and Gambit meshing tools for the numerical modeling is performed to summarize a final numerical sequence for the Darrieus rotor performance. Then, this model sequence is applied for different blade airfoils to obtain the best performance. Unsteady simulations performed for different speed ratios and based on URANS turbulent calculations using sliding mesh approach. Results show that the accuracy of ANSYS Workbench meshing is improved by using SST K-omega model but it is not recommended for other turbulence models. Moreover, this CFD procedure is used in this paper to assess the turbine performance with different airfoil shapes (25 airfoils). The results introduced new shapes for this turbine with higher efficiency than the regular airfoils by 10%. In addition, blade pitch angle has been studied and the results indicated that the zero pitch angle gives best performance.

1. Introduction

Development of wind turbine technologies allowed wind energy to perform a relevant step forward and the local production of clean electric power. It renewed the interest of vertical axis wind turbines (VAWTs) for small scale power generation [1,2]. In fact, a VAWT can operate using wind coming from any direction. Moreover, the maintenance of this type of wind generators appears to be less expansive with respect to classical turbines [3]. This paper focuses on a CFD analysis of a three-bladed Darrieus rotor using different airfoils. S1046 airfoil improved the performance of the Darriues turbine by 9%, therefore, it has been recommended by Mohamed [4]. In this work, other efficient airfoils have been introduced. Numerical analysis accuracy is very important aspect in the prediction of Darrieus turbine. The key player in the simulation is the meshing using different tools. Meshing quality and turbulence model affect the solution accuracy. Numerical analysis has been performed through a full campaign of simulations based on RANS unsteady calculations for variable values of rotor speed ratio. Speed ratio is defined as:

$$\lambda = \frac{R\omega}{V\infty} \tag{1}$$

Numerical sequence selection is very important to get accurate results from the CFD simulation. The main problem in the CFD work is the selection of the meshing accuracy, physical model and turbulence model. A lot of conflicts and confused results were obtained by the CFD worker due to misunderstanding of these selections. Therefore, the purpose of the present work is to obtain the best selection of the CFD parameters including the meshing accuracy, physical models and the turbulence models to get accurate results from the CFD simulation of Darrieus turbine.

2. State of art of numerical investigations

Most complex phenomena in the field of Computational Fluid Dynamics (CFD) are associated with the simulation of the flow past rotating blades. In addition, the aerodynamics of the Darrieus turbine is deeply influenced by the phenomenon of dynamic stall [5]. Mohamed [4] improved the design performance of H-rotor Darrieus turbine for wind energy conversion. For this purpose, 20 different symmetric and non-symmetric airfoils have been investigated by two-dimensional Computational Fluid Dynamics. Moreover, Mohamed [4] proved that the optimal configuration of H-rotor Darrieus turbine involving S-1046 appears to be very promising for wind energy generation, in particular in urban areas.

* Corresponding author. Tel.: +20 1126060364, fax: +20 2 2633 2398.
E-mail addresses: moh75202@yahoo.de, mohamed_ibrahim07@m-eng.Helwan.edu.eg (M.H. Mohamed).

Peer review under responsibility of Karabuk University.

http://dx.doi.org/10.1016/j.jestch.2014.08.002

Please cite this article in press as: M.H. Mohamed, et al., CFD analysis for H-rotor Darrieus turbine as a low speed wind energy converter, Engineering Science and Technology, an International Journal (2014), http://dx.doi.org/10.1016/j.jestch.2014.08.002

Ferreira et al. [6] focused on the numerical simulation of a single-bladed VAWT through the comparison with experimental measurements and PIV data. This demonstrated the DES model which was able to provide a good representation of the development of dynamic stall. Wang and Tao [7] also performed a two-dimensional numerical investigation of the phenomenon of deep dynamic stall for a low Reynolds number flow over a NACA 0012. They compared k-ω SST model with low Reynolds number correction and the v2-f model. They found that the RANS approach was good for fast design or research of low Reynolds number airfoils. Kumar et al. [8] suggested a low Reynolds number VAWT design and optimization procedure based on both CFD and BEM (The Boundary Element Method) calculations. Castelli et al. [9,10] presented a model for the evaluation of rotor performance and aerodynamic forces on a single-bladed helical VAWT. Moreover, they also introduced a validation study for a CFD code for a Darrieus micro-VAWT. Castelli and Benini [11] presented again a two dimensional CFD analysis of the effect of airfoil thickness on a straight-bladed Darrieus-type VAWT. They performed complete simulations based on full RANS unsteady calculations on a three-bladed rotor for two different blade profiles; NACA 0012 and NACA 0021.

Mohamed [13] improved the self-starting capability of an H-rotor Darrieus turbine for wind energy conversion. The effect of using the hybrid system between the drag and lift types of VAWTs was investigated numerically and experimentally. Hybrid system was studied to check the self-starting capability and the results indicated that the hybrid system improved the self-starting capability of Darrieus turbine. The aero-acoustics from the Darrieus rotor have evaluated also by Mohamed [14].

Guerri et al. (2007) [15] and Chen and Zhou (2009) [16] analyzed the flow around a rotating VAWT using Reynolds Averaged Navier Stokes (RANS) solver in 2-D simulation. PISO discretization scheme with SST K-omega model was utilized to obtain the flow details near the wall of the blades. Sliding mesh technique was used to make a moving mesh. NACA 0018 airfoil type was chosen in both studies. Guerri et al. (2007) [15] calculated the horizontal and vertical component of the forces acting on the airfoil to determine the value of the total torque generated by VAWT. Whereas, Chen and Zhou (2009) [16] reported the moment coefficient.

Howell et al. (2009) [17] and Claessens (2006) [18] performed experimental and computational studies on 2-D and 3-D Darruies turbine models at different Reynolds numbers. They obtained 3-D computational results in a good agreement with the experiments. Effect of surface roughness was also taken into consideration. Claessens (2006) [18] studied the effect of Reynolds number, airfoil thickness and speed ratio with different airfoil shapes; NACA 0012, NACA 0015, NACA 0018, and NACA 0021. Sabaeifard et al. [19] tried to determine the VAWTs optimal configuration through CFD simulations. They studied DUW airfoil effects on H-Darrieus wind turbine efficiency comparing with a classical airfoil (NACA 0018). Ponta et al. [20] used more complex design where the blades follow oval-trajectory at variable setting-angles. This new design didn't show any performance improvements relative to classical circular-trajectory Darrieus.

All the discussed research projects in the present review have tried to understand and improve the performance as well as self-starting of Darrieus turbine, considering either the conventional geometry or slight modifications.

It can be finally concluded that:

- There is a renewed interest for Darrieus turbines in the recent year;
- Many small modifications and improvements have been achieved in the literature for the efficiency or some specific characteristics (e.g., self-starting capability);
- Nevertheless, an accurate CFD modeling of this system has not been realized up to now. Therefore, it would be very interesting in the present study to include CFD accuracy check and study of new airfoil shapes as well as pitch angle effect.

3. CFD domain characteristics

The numerical investigation is used for the aerodynamic behavior of a three-bladed Darreius vertical axis wind turbine characterized. This turbine consists of S1046 airfoil (as started airfoil) with solidity ($\sigma = Nc/2R$) equals 0.1. Wind speed at computational domain entrance has been kept constant and equals to 5 m/s. The angular velocity of the turbine (rotating zone) is varied to evaluate the turbine performance. Table 1 shows the geometrical and kinematic features of the tested rotor, while in Table 2, the main flow field characteristics are illustrated.

3.1. Description of the numerical flow field

Darrieus turbine operates in open field conditions, so it is necessary to consider a large domain, to avoid solid blockage. Fig. 1 displays the main geometrical features of the computational domain. The appropriate size of the computational domain has been investigated to eliminate the effect of the domain size on the results. A computational domain is a square domain of size $2L \times 2L$, it has been considered in the CFD computation. Mohamed et al. [12] indicated that the smaller domains are associated with a large variation of the rotor coefficient. This demonstrates that the computational domain should extend at least over 20 times the rotor radius in each direction. In a smaller domain, the boundary conditions influence the results in an inappropriate manner. Therefore, the domain (25 D) as shown in Fig. 1 has been retained for all further computations in this paper.

Inlet has been set as a velocity inlet, with a constant wind velocity profile of 5 m/s, while, outlet has been set as a pressure outlet with atmospheric pressure value. Two symmetry boundary conditions have been used for the two side boundaries. To ensure the continuity of the flow field, the circumference around the turbine rotational axis was set as an interface. The inner zone of the flow field is named as turbine zone and also is set as interface to ensure mesh linkage between domain and turbine. Turbine zone is characterized by a moving mesh and it is revolving at the same angular velocity of the rotor. Fig. 2 shows the main dimensions and the boundary conditions of the rotating zone (turbine). All the blade profiles inside the rotating zone rotate in circle of 2000 mm diameter while the rotating zone is 1.25 times the diameter.

3.2. Domain meshing

A paved (Quad Dominant) mesh has been chosen for the whole computational domain in both ANSYS (Fig. 3) and GAMBIT (Fig. 4) meshing tools. This type of mesh is selected in order to reduce the

Table 1
Main geometrical features of the analyzed rotor.

Denomination	Value
Rotor diameter (D) [mm]	2000
Rotating zone diameter	1.25D
Rotor height (H) [m]	1
Blade section	S1046
Blade chord (c) [mm]	70
Number of blades (n) [-]	3
Turbine solidity (σ) [-]	0.1

Please cite this article in press as: M.H. Mohamed, et al., CFD analysis for H-rotor Darrieus turbine as a low speed wind energy converter, Engineering Science and Technology, an International Journal (2014), http://dx.doi.org/10.1016/j.jestch.2014.08.002

Table 2
Main Characteristics of the simulated flow field.

Denomination	Value
Pressure [Pa]	101325
Density (ρ) [kg/m3]	1.225
Inlet velocity (V_∞) [m/s]	5

computational time and increasing the accuracy in spite of increasing the preparation time of the CFD simulations. The mesh on both sides of the interface (domain and turbine) has approximately the same characteristics cell size to obtain faster convergence.

Being the area close to the blade profiles, great attention where the computational grids have been constructed from lower topologies to higher ones and adopting appropriate size. Clustering grid points near the leading edge and the trailing edge of the blade profile is to capture the physics and improves the CFD code capability. Figs. 5 and 6 represent the mesh near wall using ANSYS and GAMBIT, respectively.

4. Numerical solution

A finite volume CFD solver ANSYS FLUENT is used in this work, that implements Reynolds averaged Navier–Stokes equations. The

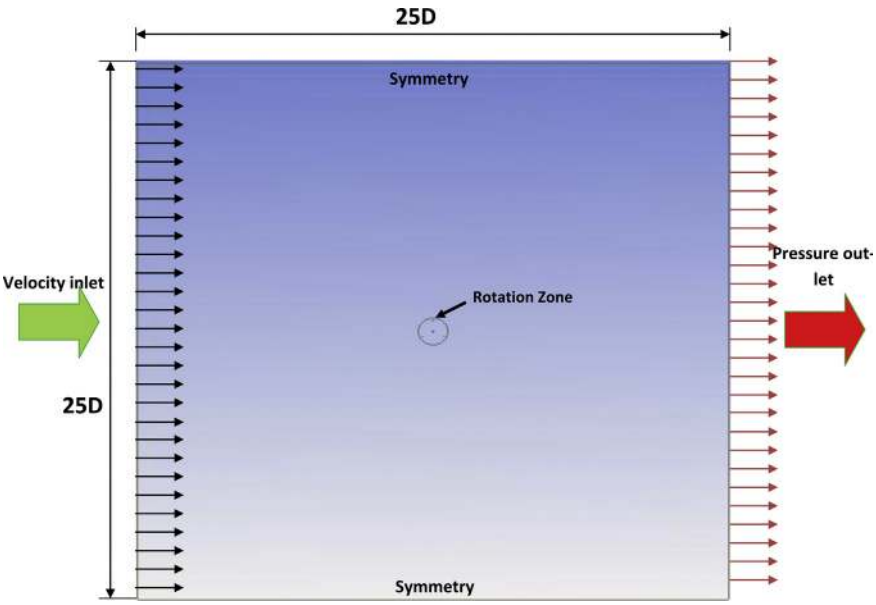

Fig. 1. Geometrical features and main dimensions of the computational domain.

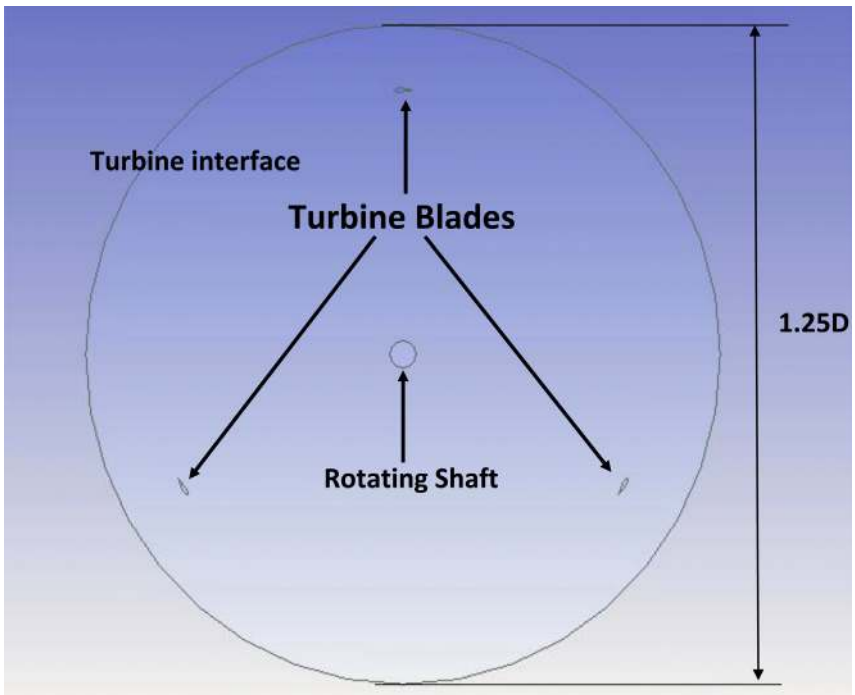

Fig. 2. Scheme of rotating zone area.

Please cite this article in press as: M.H. Mohamed, et al., CFD analysis for H-rotor Darrieus turbine as a low speed wind energy converter, Engineering Science and Technology, an International Journal (2014), http://dx.doi.org/10.1016/j.jestch.2014.08.002

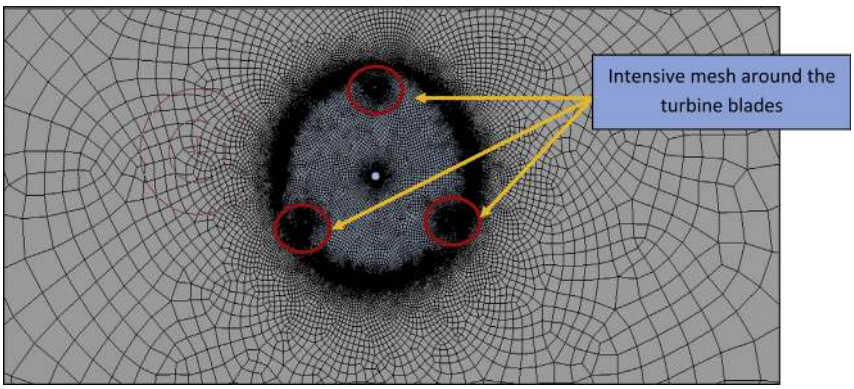

Fig. 3. ANSYS mesh for a three-bladed VAWT.

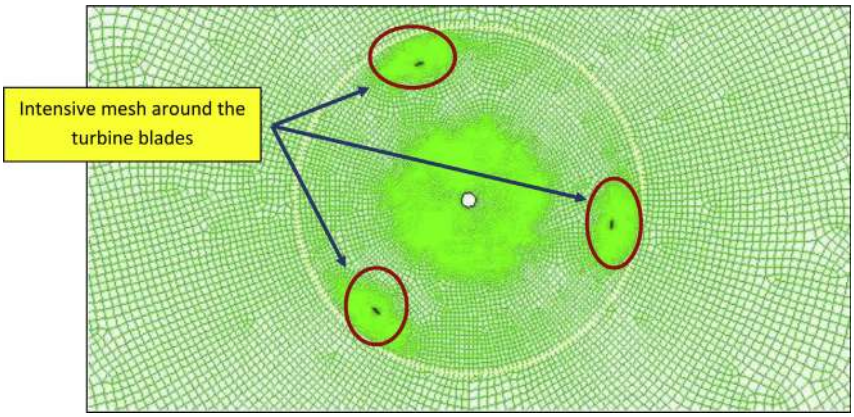

Fig. 4. GAMBIT mesh for a three-bladed VAWT.

fluid has been assumed to be incompressible since the inlet velocity equals 5 m/s. The hypothesis of incompressible flow is consistent taking into account the relative speed to the blade. It does not exceed 45 m/s and it is acceptable (Ma < 0.15). By studying the effect of time step size on torque coefficient using 0.001, 0.002, 0.004 and 0.005 s time step size, it is observed that is the change in torque coefficient doesn't exceed 5%. In addition, same study performed for the maximum number of iteration as the the calculation performed using 50, 70, 80 and 90 maximum number of iteration; the change in torque coefficient doesn't exceed 1%.

The time step size is set to be 0.005 by performing the computations on 7 revolutions with 70 maximum number of iteration. As a global convergence criterion, each simulation has been run until instantaneous torque coefficient is less than 1% compared with the relative values of the previous period. Residuals convergence criterion for each physical time step has been set to 10^{-5}. Furthermore, Courant number can be calculated for 0.005 time step size to ensure that is within the acceptable range. As the minimum cell size is 7.07×10^{-3} ms, Courant number will be about 3.5 which is acceptable for such cases. The selected solver is pressure based, well suited to compute an incompressible flow field. Two turbulence models have been checked in this step of work, Realizable k–ε and the SST k–ω. These two models are recommended by the CFD worker for the rotating zones. The power coefficient shown in the figures is an average over an entire revolution.

The Realizable k–ε model has been adopted for viscous computations. This model differs from the Standard k–ε in two points; 1) it contains a new formulation for the turbulent viscosity and 2) a new transport equation for the dissipation rate ε has been derived from an exact equation for the transport of the mean-square vorticity fluctuations. One of the benefits of the Realizable k–ε model is that it provides superior performances for flows involving rotation, boundary layers under strong adverse pressure gradients, separation and recirculation.

SST k–ω turbulence model is a two-equation eddy-viscosity model which has become very popular. Usage of a k–ω formulation in the inner parts of the boundary layer makes the model directly usable all the way down to the wall through the viscous sub-layer. Hence, the SST k–ω model can be used as a low-Re turbulence model without any extra damping functions. SST formulation also switches to a k–ε behavior in the free-stream to avoid the common

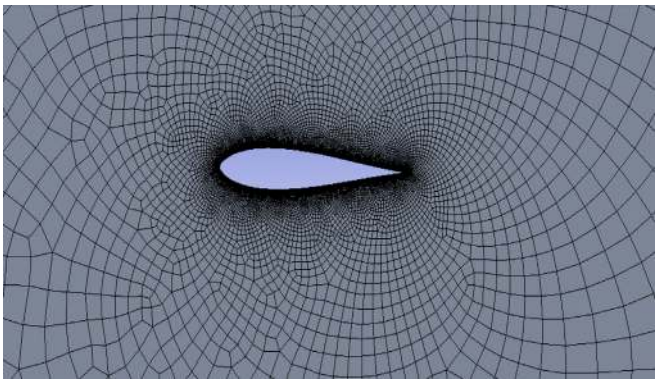

Fig. 5. Grid at airfoil section using ANSYS.

Please cite this article in press as: M.H. Mohamed, et al., CFD analysis for H-rotor Darrieus turbine as a low speed wind energy converter, Engineering Science and Technology, an International Journal (2014), http://dx.doi.org/10.1016/j.jestch.2014.08.002

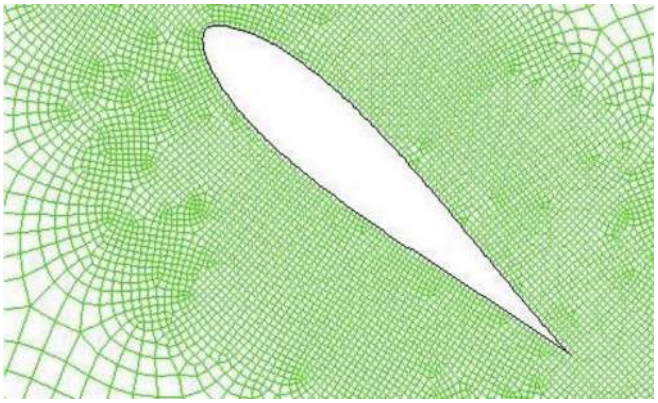

Fig. 6. Grid at airfoil section using GAMBIT.

k–ω problem. SST model is too sensitive to the inlet free-stream turbulence properties. So, firstly the computations are taken place using Realizable k–ε for both models meshed by ANSYS and GAMBIT and compare it with SST k–ω results. The computations use SST k–ω for ANSYS model by keeping the a fine near-wall mesh capable of resolving the viscous sub-layer ($y^+ < 5$) and compare it with the GAMBIT model performed by Realizable k–ε.

5. Mathematical methodology

ANSYS FLUENT can handle both steady-state and transient analyses, and has several different options for modeling turbulence. Conservation of both mass and momentum is solved in all fluid flow cases, and in compressible flow or heat transfer cases. Consider a control volume which encloses a specified mass of fluid in a steady-state flow field. Also consider a control surface around this volume, through which a certain mass of fluid enters and exits over a specific interval of time. If the flow is steady-state, these quantities are equal; therefore, there is no change in mass of the volume. This is the principle of continuity.

The continuity equation for unsteady, compressible flow is.

$$\frac{\partial(\rho v_x)}{\partial x}+\frac{\partial(\rho v_y)}{\partial y}+\frac{\partial(\rho v_z)}{\partial z}+\frac{\partial \rho}{\partial t}=0 \tag{2}$$

where v_x, v_y, and v_z are the fluid velocities in the x, y, and z directions, respectively, and ρ is the density of the fluid. This equation states that the time rate at which mass increases within the control volume is equal to the net influx of mass across the control surface. Conservation of momentum can be written as

$$\frac{\partial}{\partial t}(\rho\vec{v})+\nabla\cdot(\rho\vec{v}\,\vec{v})=-\nabla p+\nabla\cdot(\vec{\tau})+\rho\vec{g}+\vec{F} \tag{3}$$

where$\rho\vec{g}$ and $\vec{F}$ are the gravitational and body forces, the stress tensor, $\overline{\tau}$ is.

$$\overline{\tau}=\mu\left[\left(\nabla\vec{v}+\nabla\vec{v}^{T}\right)-\frac{2}{3}\nabla\cdot\vec{v}I\right] \tag{4}$$

Fluid behavior can be characterized in terms of the fluid properties velocity vector u (with components u, v, and w in the x, y, and z directions), pressure p, density ρ, viscosity μ, heat conductivity k, and temperature T. Changes in these fluid properties can occur over space and time. Using CFD, these changes are calculated for small elements of the fluid, following the conservation laws of physics listed above. The changes are due to fluid flowing across the boundaries of the fluid element and can also be due to sources within the element producing changes in fluid properties.

Since it would be computationally prohibitive to model very small scale and high frequency fluctuations in fluid velocity seen in turbulent flow in production environments, time averaged methods of simulating turbulence effects have been derived. In these models, terms are introduced to simulate the average turbulent flow field, so that the small scale turbulent behavior does not have to be calculated explicitly by the Navier Stokes equations. Instead, transport equations are solved in order to bring the model to closure and model the full range of turbulent flow scales. These are called Reynolds-average Navier Stokes (RANS) turbulence models which significantly reduce the processing power required and make turbulence modeling practical for a wide range of turbulent flow problems. In turbulence models that involve Reynolds averaging, the exact Navier stokes flow solution is broken down into its varying and time averaged components. The general form of any scalar flow property can be given as

$$\phi=\overline{\phi}+\phi', \tag{5}$$

where $\overline{\phi}$ is the mean property value, and ϕ' is the varying value. If the time averaged values of the flow variables are substituted into the standard Navier Stokes equations, the Reynolds-averaged Navier–Stokes equations can be obtained:

$$\frac{\partial}{\partial t}(\rho u_i)+\frac{\partial}{\partial x_j}(\rho u_i\rho u_j)=-\frac{\partial p}{\partial x_i}+\frac{\partial}{\partial x_j}\left[\mu\left(\frac{\partial u_i}{\partial x_j}+\frac{\partial u_j}{\partial x_i}-\frac{2}{3}\delta_{ij}\frac{\partial u_l}{\partial x_l}\right)\right]+\frac{\partial}{\partial x_j}\left(-\rho\overline{u_i'u_j'}\right) \tag{6}$$

Two-equation RANS turbulence models use the Boussinesq hypothesis which states that the transfer of momentum generated by turbulent eddies can be modeled by an eddy viscosity, μ_t. The theory states that the Reynolds stress tensor, τ_{ij} is proportional to the rate of strain tensor$\overline{S}_{ij}$, defined as

$$\overline{S}_{ij}=\frac{1}{2}\left(\frac{\partial\overline{u}_i}{\partial x_j}+\frac{\partial\overline{u}_j}{\partial x_i}\right). \tag{7}$$

They can be combined as

$$\tau_{ij}=2\mu_t 2\overline{S}_{ij}-\frac{2}{3}k\delta_{ij}. \tag{8}$$

This can also be written as

$$-\rho\overline{u_i'u_j'}=\mu_t\left(\frac{\partial u_i}{\partial x_j}+\frac{\partial u_j}{\partial x_i}\right)-\frac{2}{3}\left(\rho k+\mu_t\frac{\partial u_k}{\partial x_k}\right)\delta_{ij}. \tag{9}$$

Boussinesq assumption provides a method of calculating the turbulent viscosity at a low computational cost. However, its main disadvantage that the Reynolds stress tensor is proportional to the strain rate tensor. This is not strictly true and is in fact invalid for a range of flows including those with strong accelerations or high curvature. Models have been developed which attempt to address this shortcoming, such as the Realizable k–epsilon and SST k–omega models which are described below.

5.1. Realizable k–epsilon turbulence model

A member of the k–ε family of turbulence models, k–ε Realizable, was used for rotating zones. Advantages of the k–ε Realizable turbulence model over the standard k–ε turbulence model include improved performance in flows with recirculation, strong pressure gradients, flow separation, and the non-reliance on an assumed

Please cite this article in press as: M.H. Mohamed, et al., CFD analysis for H-rotor Darrieus turbine as a low speed wind energy converter, Engineering Science and Technology, an International Journal (2014), http://dx.doi.org/10.1016/j.jestch.2014.08.002

relationship between the Reynolds stress tensor and the strain rate tensor.

The transport equations for k and ε in the Realizable k–ε model are given as.

$$\frac{\partial}{\partial t}(\rho k)+\frac{\partial}{\partial x_j}(\rho k u_j)=\frac{\partial}{\partial x_j}\left[\left(\mu+\frac{\mu_t}{\sigma_k}\right)\frac{\partial k}{\partial x_j}\right]+G_k+G_b-\rho\varepsilon-Y_M+S_k \tag{10}$$

and

$$\frac{\partial}{\partial t}(\rho\varepsilon)+\frac{\partial}{\partial x_j}(\rho\varepsilon u_j)=\frac{\partial}{\partial x_j}\left[\left(\mu+\frac{\mu_t}{\sigma_\varepsilon}\right)\frac{\partial \varepsilon}{\partial x_j}\right]+\rho C_1 S\varepsilon-\rho C_2\frac{\varepsilon^2}{k+\sqrt{\nu\varepsilon}}+C_{1\varepsilon}\frac{\varepsilon}{k}C_3 G_b+S_\varepsilon \tag{11}$$

where

$$C_1=\max\left[0.43,\frac{\eta}{\eta+5}\right],\ \eta=S\frac{k}{\varepsilon}\ \text{and}\ S=\sqrt{2S_{ij}S_{ij}}$$

Major difference in the form of the Realizable k–ε model versus that of the standard k–ε model is that in the determination of C_μ is not a constant. It is instead calculated from.

$$C_\mu=\frac{1}{A_0+A_S\frac{kU^*}{\varepsilon}} \tag{12}$$

where

$$U^*=\sqrt{S_{ij}S_{ij}+\tilde{\Omega}_{ij}\tilde{\Omega}_{ij}} \tag{13}$$

and

$$\tilde{\Omega}_{ij}=\Omega_{ij}-2\varepsilon_{ijk}\omega_k \qquad \Omega_{ij}=\overline{\Omega}_{ij}-\varepsilon_{ijk}\omega_k. \tag{14}$$

5.2. SST k–omega turbulence model

Shear-stress transport (SST) k–omega turbulence model is a type of hybrid model, combining two models in order to calculate flow in the near-wall region. It was designed in response to the problem of the k–*epsilon* model's unsatisfactory near-wall performance for boundary layers with adverse pressure gradients. It uses a standard k–ε model to obtain flow properties in the free-stream (turbulent) flow region far from the wall, while using a modified k–ε model near the wall using the turbulence frequency ω as a second variable instead of turbulent kinetic energy dissipation term ε. It is expected that the boundary layer flow has a strong

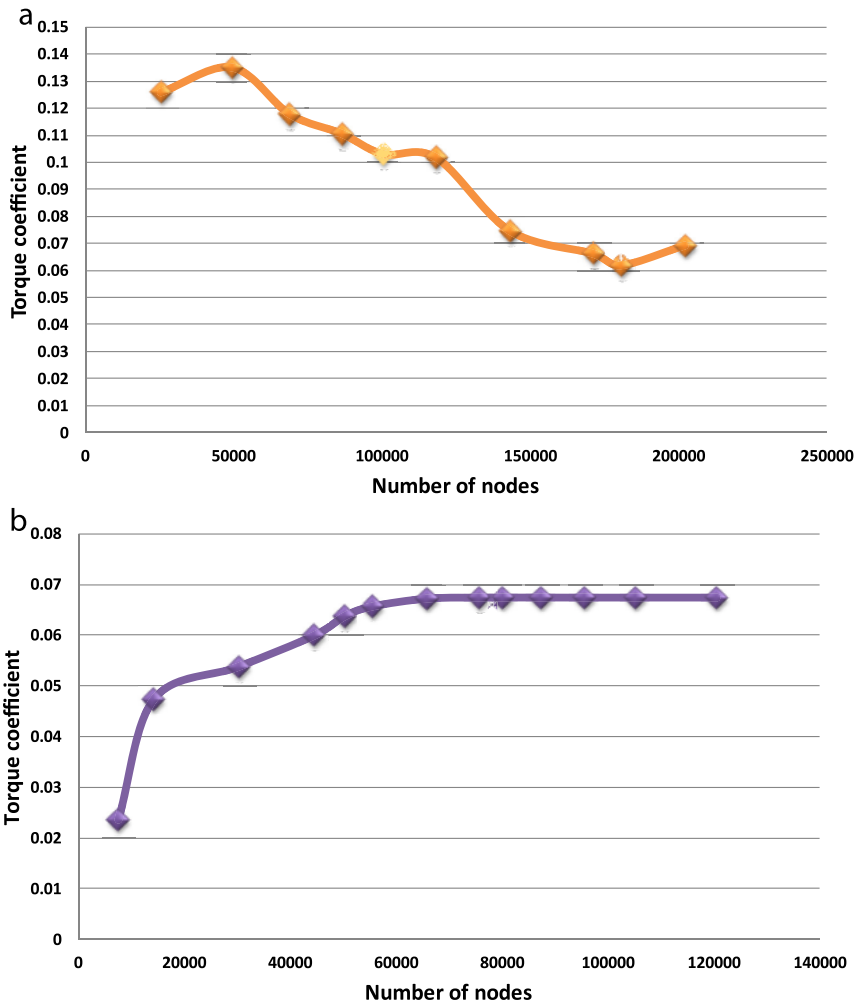

Fig. 7. a. ANSYS meshed model by using Realizable k–ε turbulence model b. GAMBIT meshed model by using Realizable k–ε turbulence model.

Please cite this article in press as: M.H. Mohamed, et al., CFD analysis for H-rotor Darrieus turbine as a low speed wind energy converter, Engineering Science and Technology, an International Journal (2014), http://dx.doi.org/10.1016/j.jestch.2014.08.002

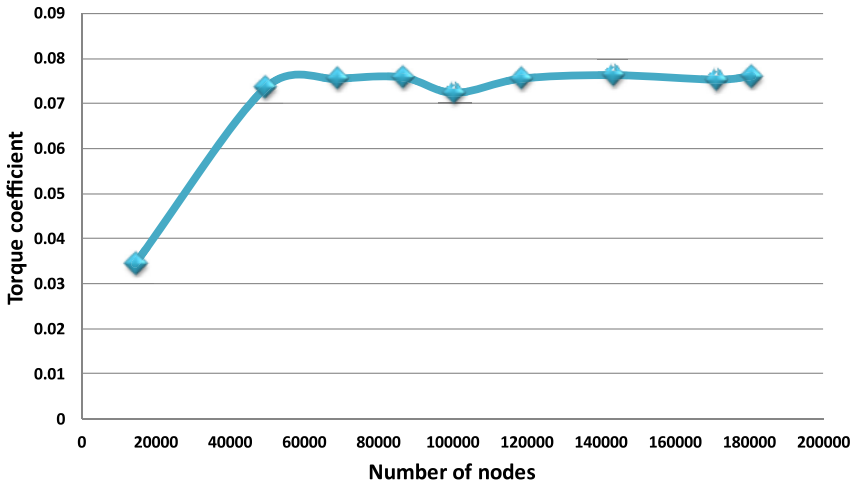

Fig. 8. ANSYS meshed model by using SST k–ω turbulence model.

influence on the results, and properly modeling this near-wall flow could be important for accuracy of the calculations. Therefore, SST *k–omega* turbulence model has also been chosen for CFD simulations in this project. This SST *k–omega* model is similar to the k–ε turbulence model, but instead of ε as the second variable, it uses a turbulence frequency variable omega, which is expressed as $\omega = \varepsilon/k$ [s^{-1}]. SST *k-omega* model calculates Reynolds stresses in the same way as in the *k–epsilon* model.

The transport equation for turbulent kinetic energy k for the k-ω model is:

$$\underset{\text{(I)}}{\frac{\partial(\rho k)}{\partial t}} + \underset{\text{(II)}}{\frac{\partial}{\partial x_i}(\rho U_i k)} = \underset{\text{(III)}}{\frac{\partial}{\partial x_i}\left[\left(\mu + \frac{\mu_t}{\sigma_k}\right) grad(k)\right]} + \underset{\text{(IV)}}{P_k} - \underset{\text{(V)}}{\beta^* \rho k \omega} \tag{15}$$

where $P_k = \left(2\mu_t \frac{\partial U_i}{\partial x_j} \cdot \frac{\partial U_i}{\partial x_j} - \frac{2}{3}\rho k \frac{\partial U_i}{\partial x_j}\delta_{ij}\right)$

The terms (I)–(V) in Equation (15), can be defined as the following:

(I)	Transient term	Accumulation of k (rate of change of k)
(II)	Convective transport	Transport of k by convection
(III)	Diffusive transport	Turbulent diffusion transport of k
(IV)	Production term	Rate of production of k
(V)	Dissipation	Rate of dissipation of k

σ_k and β^* are equation constants.

The transport equation for turbulent frequency ω for the k–ω model is:

$$\underset{\text{(I)}}{\frac{\partial \rho\omega}{\partial t}} + \underset{\text{(II)}}{\frac{\partial}{\partial x_i}(\rho U_i \omega)} = \underset{\text{(III)}}{\frac{\partial}{\partial x_i}\left[\left(\mu + \frac{\mu_t}{\sigma_{\omega,1}}\right) grad(\omega)\right]} + \underset{\text{(IV)}}{\gamma_2\left(2\rho \frac{\partial U_i}{\partial x_j} \cdot \frac{\partial U_i}{\partial x_j} - \frac{2}{3}\rho\omega \frac{\partial U_i}{\partial x_j}\delta_{ij}\right)} - \underset{\text{(V)}}{\beta_2 \rho \omega^2} + \underset{\text{(VI)}}{2\frac{\rho}{\sigma_{\omega,2}\omega}\frac{\partial k}{\partial x_k}\frac{\partial \omega}{\partial x_k}} \tag{16}$$

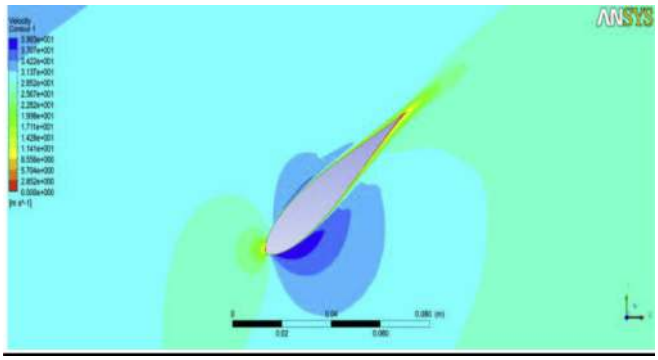

Fig. 9. Absolute velocity contours [m/s] around the airfoil for ANSYS meshed model by using SST k–ω turbulence model.

where $\sigma_{\omega,1}$, γ_2, β_2, and $\sigma_{\omega,2}$ are constants.

The general description for each of the terms in Equation 15(I) to (V) are the usual terms for accumulation, convection, diffusion, production, and dissipation of ω. Last term (VI) is called a 'cross-diffusion' term, an additional source term, and has a role in the transition of the modeling from ε to ω.

6. Results and discussion

Torque coefficient and power coefficient are used to assess the mesh quality and stability of used turbulence model. These coefficients are represented by the following:

$$C_m = \mathrm{T} \Big/ \left(\tfrac{1}{2}\rho \cdot A \cdot V_\infty^2 \cdot R\right) \tag{17}$$

Please cite this article in press as: M.H. Mohamed, et al., CFD analysis for H-rotor Darrieus turbine as a low speed wind energy converter, Engineering Science and Technology, an International Journal (2014), http://dx.doi.org/10.1016/j.jestch.2014.08.002

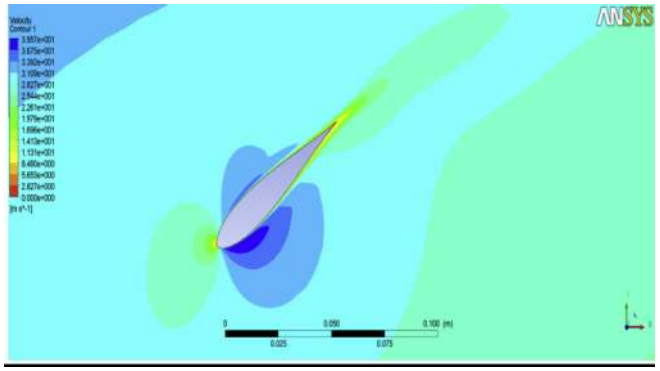

Fig. 10. Absolute velocity contours [m/s] around the airfoil for ANSYS meshed model by using Realizable $k-\varepsilon$ turbulence model.

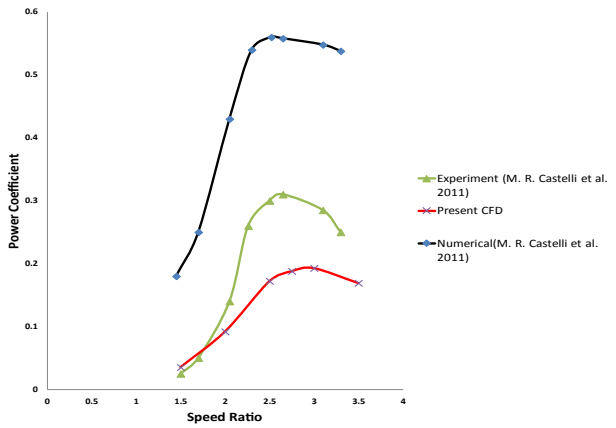

Fig. 11. Validation of computational model using NACA 0021 airfoil, compared to a published experimental and CFD results for a Darrieus turbine [21].

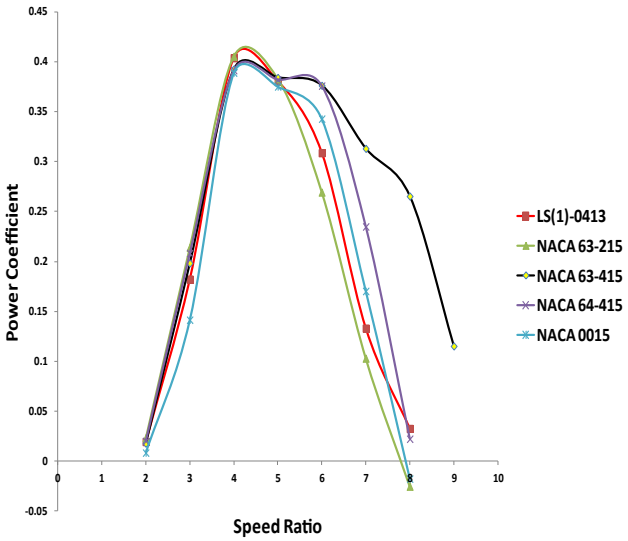

Fig. 13. Power coefficient as a function of tip speed ratio for the best five Blade's sections.

$$C_p = P \Big/ \left(\tfrac{1}{2}\rho \cdot A \cdot V_\infty^3\right) \tag{18}$$

As a function of speed ratio for a given blade section (S1046), it clearly appears in Fig. 7a that using Realizable $k-\varepsilon$ as the turbulence model for the model meshed by ANSYS gives unstable solution over a wide range of number of nodes. The solution is grid dependent in spite of reaching a great number of nodes up to 202426 nodes. By using the Realizable $k-\varepsilon$ as the turbulence model for the model meshed by GAMBIT, Fig. 7b shows that it gives as stable solution over a wide range of number of nodes and it can use much less number of nodes and save the computational cost. The solution is

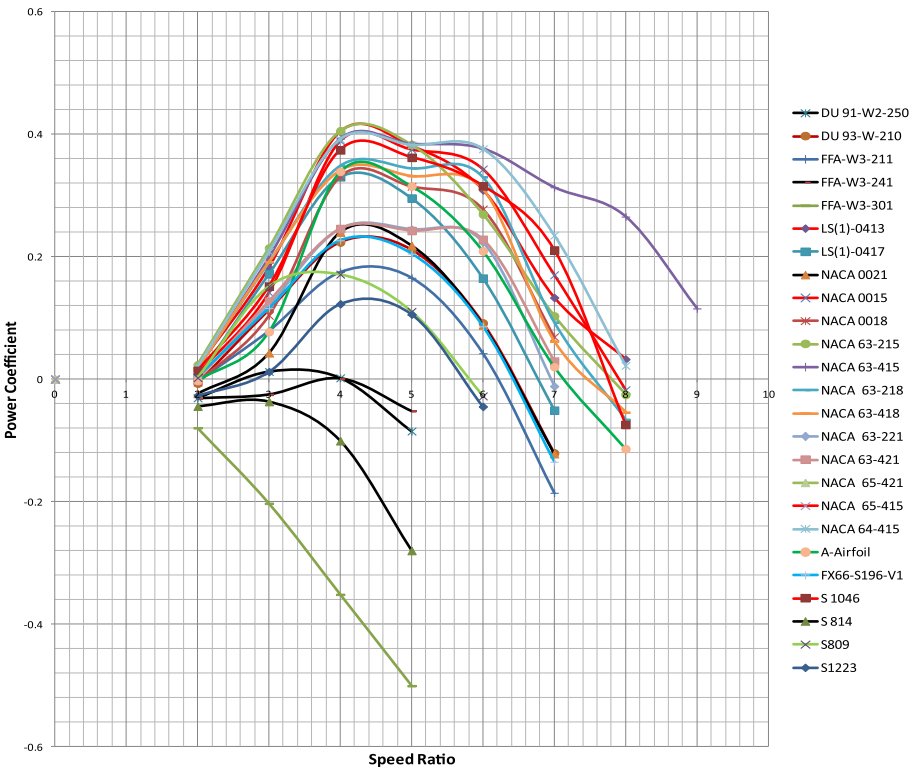

Fig. 12. Power coefficient as a function of tip speed ratio for the 25 considered blade sections.

Please cite this article in press as: M.H. Mohamed, et al., CFD analysis for H-rotor Darrieus turbine as a low speed wind energy converter, Engineering Science and Technology, an International Journal (2014), http://dx.doi.org/10.1016/j.jestch.2014.08.002

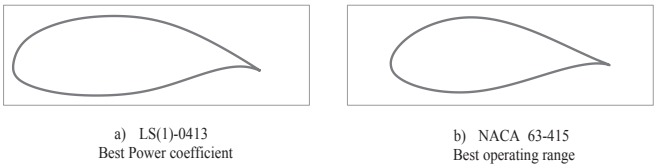

a) LS(1)-0413
Best Power coefficient

b) NACA 63-415
Best operating range

Fig. 14. Best airfoils form the performance point of view; a) best power coefficient, and b) best operating range.

grid independent and the small variation is due to numerical error with maximum variation in solution of approximately 3%.

By enhancement the mesh wall function, so it suitable to use SST $k-\omega$ as the turbulence model for the model meshed by ANSYS which doesn't give reliable solution using Realizable $k-\varepsilon$ as the turbulence model. Fig. 8 shows that using SST $k-\omega$ gives stable solution over wide range of number of nodes with maximum solution variation about 5%. Knowing that if will works on much greater number of nodes than used in GAMBIT where SST $k-\omega$ model needs intensive mesh near walls to keep $y^+ < 5$. So it needs higher computational cost than in GAMBIT as we reached $y^+ = 3.7$.

Figs. 9 and 10 compare the absolute velocity contours for the considered rotor blade sections, for models meshed using ANSYS and modeled using SST $k-\omega$ turbulence model and Realizable $k-\varepsilon$ turbulence model, respectively. A larger recirculation zone is clearly visible at the trailing edge of the Realizable $k-\varepsilon$ turbulence model. This is determining a decreased lift to drag ratio and a consequent loss of energy. This means that the SST $k-\omega$ turbulence model is better than Realizable $k-\varepsilon$ turbulence model especially near the walls. Therefore, the SST $k-\omega$ turbulence model will be retained in the rest of simulations to obtain the Darrieus rotor performance.

6.1. Turbulence model validation

Numerical turbulence model (SST $k-\omega$ turbulence model) has been validated by comparison with published experimental results and CFD for an H-rotor Darrieus turbine [11,21]. The results have been obtained by the turbulence model are shown in Fig. 11. These results give an acceptable agreement obtained between experiments and better than the CFD results of the same authors. The present CFD and the published data (Experimental and CFD, [21]) for the target function C_P are using the same rotor characteristics which selected by the authors. These results prove that present CFD procedure is more suitable for Darrieus turbine than the numerical results introduced by the authors in [21].

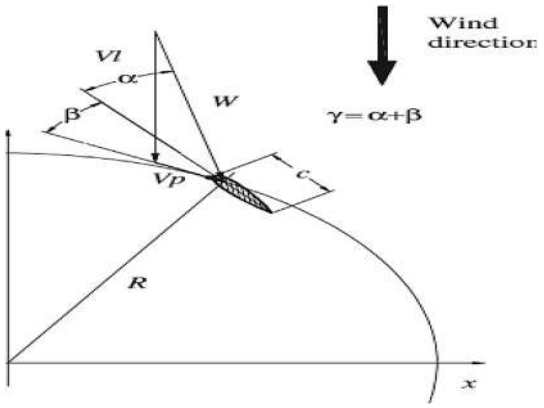

Fig. 16. Pitch angle and incidence angle definition.

6.2. Darrieus turbine performance investigation

There are several factors that performance of the wind turbine depends on, such as lift to drag ratio which is affected by airfoil shape, pitch angle, solidity, speed ratio and wind velocity. This section mainly deals the results obtained from a proper assessment of an airfoil shape and pitch angle are to maximize the power output. Torque coefficient C_m and power coefficient C_p are calculated on base of Equations (17) and (18) to evaluate turbine performance for different configurations including the changing in blade section and pitch angle.

6.2.1. Airfoil shape effect

In this section, results from the numerical study will be presented for each airfoil shape in order to obtain better performance for H-rotor Darrieus turbine. The study performed based on 25 airfoil section from different families. The names of these airfoils are NACA 63-215, NACA 63-415, NACA 63-218, NACA 63-418, NACA 63-221, NACA 63-421, NACA 64-415, NACA 65-415, NACA 65-421, NACA 0015, NACA 0018, NACA 0021, FFA-W3-211, FFA-W3-241, FFA-W3-301, A-Airfoil, DU91-W2-250, DU93-W-210, LS(1)-0413, LS(1)-0417, FX66-S196-V1, S809, S814, S104 and S1223. Most of these airfoils is recommended to use in horizontal axis wind turbines

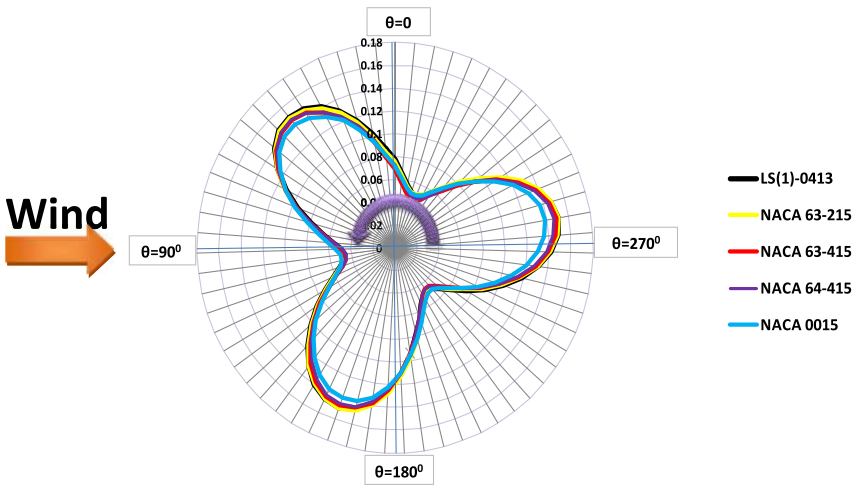

Fig. 15. Instantaneous torque coefficients for the best in class airfoils at $\lambda = 4$.

Please cite this article in press as: M.H. Mohamed, et al., CFD analysis for H-rotor Darrieus turbine as a low speed wind energy converter, Engineering Science and Technology, an International Journal (2014), http://dx.doi.org/10.1016/j.jestch.2014.08.002

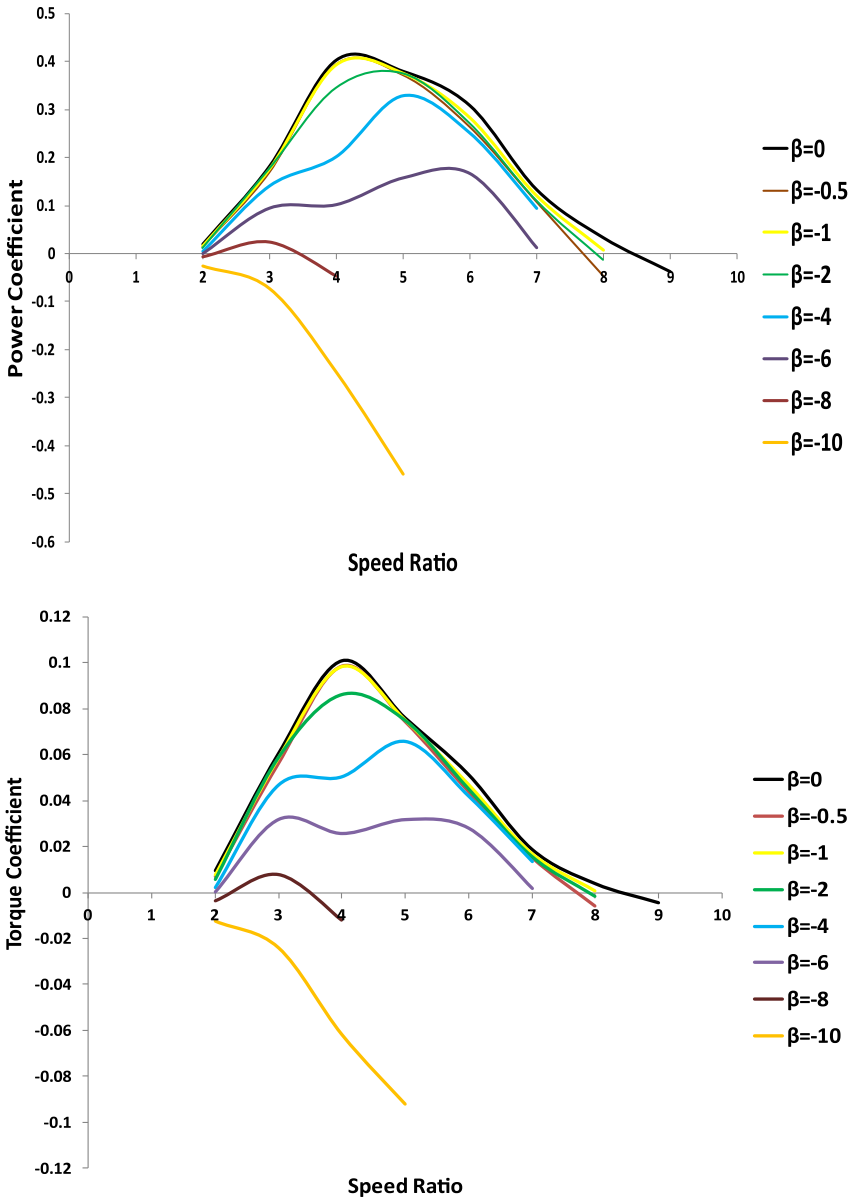

Fig. 17. Power and torque coefficient as a function of tip speed ratio for the negative pitch angles compared to zero pitch.

where they give great lift to drag ratio but never used before in the vertical axis wind turbines. So the performance of such airfoil sections is investigated to show if it is suitable for vertical axis wind turbines or not. The rest of airfoils are traditional sections for comparing it with the new sections. The geometric parameters that affect the aerodynamic performance of an airfoil include leading edge radius, mean camber line, maximum thickness, thickness distribution of the profile and the trailing edge angle.

Present work considers a typical operating range (speed ratio range) varying between 2 and 9. Due to an extremely small power output, there is no practical interest for the operating range above 9, ($\lambda > 9$). Operation below speed ratio 2 ($\lambda < 2$) means the turbine is working beyond stall conditions especially for high solidities, where the efficiency and power output rapidly decrease. Many publications recommended the range between 2 and 9 [21] and this range has been retained as well in the present study.

From the results (see Fig. 12), it is found that the best performance of Darrieus turbine is obtaind when using one of five airfoils LS(1)-0413, NACA 63-215, NACA 63-415, NACA 64-415 or NACA 0015. These airfoils perform the maximum turbine efficiencies with wide operating range over all other used airfoils Fig. 13. The investigations will completed using LS(1)-0413 as a sample from the best of class airfoils which its peak efficiency is not much lower than the one which perform maximum peak efficiency (NACA 63-215) and it performs wider operating range (speed ratio range) for the turbine, this means that the stall can be delayed by using LS(1)-0413 airfoils without losing too much efficiency. Also it was found that NACA 63-415 perform the wider operating range over the all best in class airfoil and the power coefficient relatively constant over wider range after reaching the peak which makes it preferred for some designer where it makes the control on speed ratio that perform high efficiency more easy. Also NACA 64-415 and NACA 0015 is better than LS(1)-0413 where their operating range is wider and the power coefficient relatively constant over wider range, the power coefficient is higher at speed ratio more than 5 and less than 8 but NACA 63-415 still preferred from this side of view. NACA 63-

Please cite this article in press as: M.H. Mohamed, et al., CFD analysis for H-rotor Darrieus turbine as a low speed wind energy converter, Engineering Science and Technology, an International Journal (2014), http://dx.doi.org/10.1016/j.jestch.2014.08.002

415 gives a good performance in high speed ratio; this means that the airfoil has a high lift to drag ratio on the small angle of attacks and this reason of the usage of this airfoil on the horizontal axis wind turbine. So, in general NACA 63-415 and NACA 64-415 show the best performance over the all considered airfoils (Fig. 14). Fig. 15 shows the instantaneous torque coefficient of the five airfoils at every angle during a complete revolution.

6.2.2. Pitch angle effect

In this section the effect of pitch angle variation (β) will be discussed on the turbine performance. Fig. 16 introduces a definition to the pitch angle and its relation with angle of attack and incident angle. Pitch angle affects the air incidence angle on airfoil during the rotation. Incidence angel (γ) is the sum of pitch angle and angle of attack.

To maximize the turbine efficiency using LS(1)-0413 airfoil section, an investigation is conducted in order to get the best pitch angle. This investigation covers a wide range of pitch angle, from -10^0 to $+10^0$. Figs. 17 and 18 show the effect of variation of pitch angle from zero to -10^0 and from zero to 10^0, respectively. It is found that either increase or decrease the pitch angle from zero reduces the power coefficient and narrows the operating range. This reduction in performance reaches the case of rotation in reverse direction at -10° and 10° over all the operating range where the dynamic stall increased.

Figs. 19 and 20 indicate that by varying pitch angle from zero, the average torque coefficient of the three blades decreases at every location during rotation. So, the average torque coefficient over the revolution decreases until reaching negative torque at any angle. This confirms that the best pitch configuration is at pitch angle equals to zero. Fig. 21 shows velocity distribution contours for 10^0, -10^0 and zero pitch angle cases, while Fig. 22 is the corresponding pressure contours. Either increasing or decreasing the pitch angle other than zero pitch shows a dramatic change in the pressure distribution plot. It can be seen that there is a very large low pressure region on top of the blade in case of 10^0 pitch angle and the stagnation point has been moved to the bottom of the airfoil. Inversely in case of -10° the large low pressure region appears on the bottom while the stagnation point is moved to the top. As the stagnation point displaced, at the trailing edge there are two

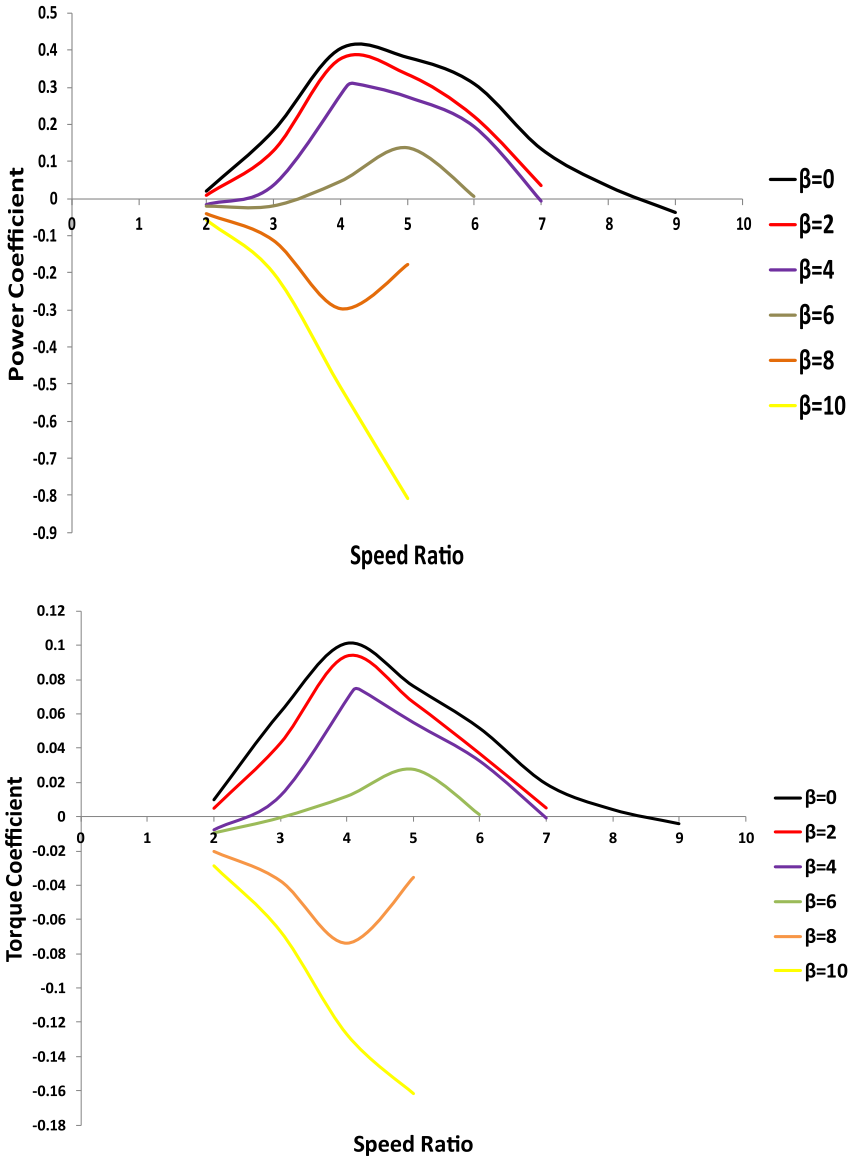

Fig. 18. Power and torque coefficient as a function of tip speed ratio for the positive pitch angles compared to zero pitch.

Please cite this article in press as: M.H. Mohamed, et al., CFD analysis for H-rotor Darrieus turbine as a low speed wind energy converter, Engineering Science and Technology, an International Journal (2014), http://dx.doi.org/10.1016/j.jestch.2014.08.002

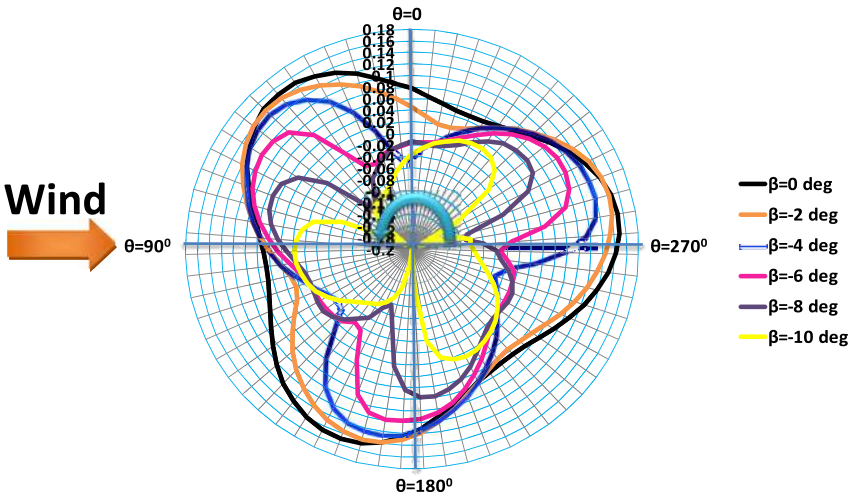

Fig. 19. Instantaneous torque coefficients for different negative and zero pitch angle at $\lambda = 4$.

streams traveling at different velocities. This causes a starting vortex at the trailing edge and grows as stagnation point moves either on suction or on pressure side.

7. Conclusions

Numerical procedure relying on the Realizable $k-\varepsilon$ turbulence and SST $k-\omega$ models can be employed for a quantitative analysis of the performance of H-Darriues turbine, provided a sufficiently fine grid and sufficiently large computational domain are used. The behavior of CFD simulation based on H-rotor Darrieus turbine is affected by the meshing tool. If the domain is meshed using ANSYS, it is recommended to intense mesh near wall and use SST $k-\omega$ to give reliable solution. It needs much more computational cost as well as it should be checked the viscous sub-layer (y^+). Moreover, if the model has been installed and meshed by GAMBIT tool,

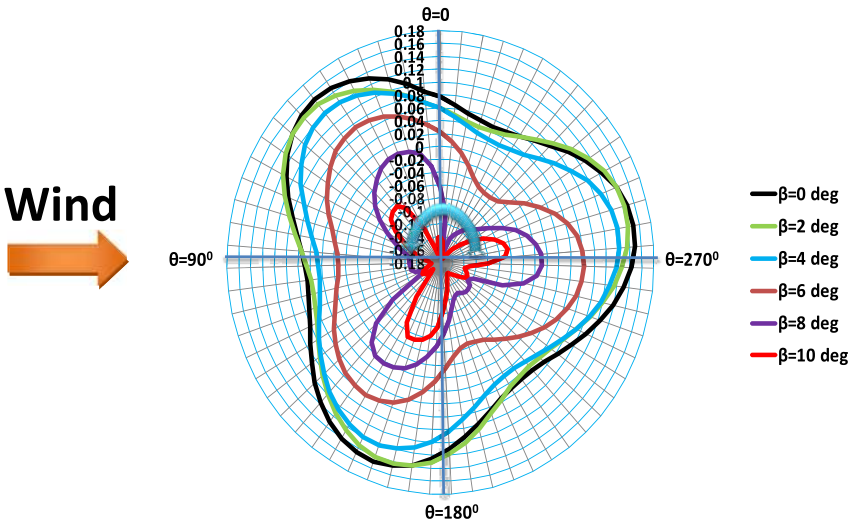

Fig. 20. Instantaneous torque coefficients for different positive and zero pitch angle at $\lambda = 4$.

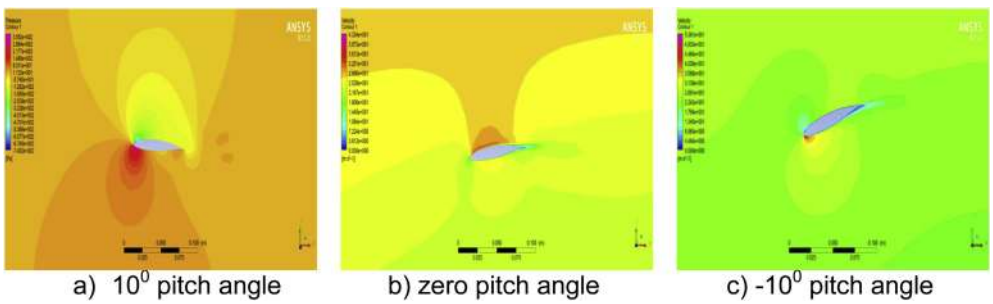

Fig. 21. Velocity contours for LS(1)-0413 profile; a) zero pitch, b) -10^0 pitch and c) 10^0 pitch angle at $\lambda = 4$.

Please cite this article in press as: M.H. Mohamed, et al., CFD analysis for H-rotor Darrieus turbine as a low speed wind energy converter, Engineering Science and Technology, an International Journal (2014), http://dx.doi.org/10.1016/j.jestch.2014.08.002

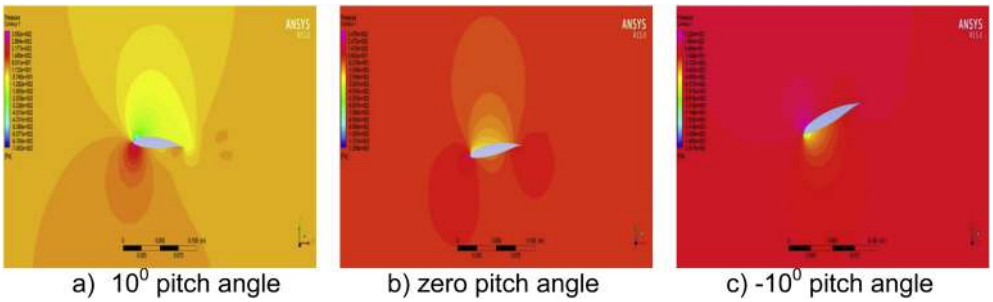

Fig. 22. Static pressure contours for LS(1)-0413 profile; a) zero pitch, b) -10^0 pitch and c) 10^0 pitch angle at $\lambda = 4$.

Realizable $k-\varepsilon$ should be used as the turbulence model which doesn't need wall treatment so less computational cost. 25 airfoils based Darrieus rotor has been investigated for several values of speed ratio in order to obtain the best possible performance. LS(1)-0413 airfoil cross section gives power coefficient equals 0.415 with an increase around 10% compared to NACA 0018. However, NACA 63-415 introduces wider operating range compare to all the airfoils. The effect of pitch angle variation is investigated from -10^0 to $+10^0$ using one of the best airfoils. It is concluded that by increasing or decreasing pitch angle from zero the performance start to decay until reaching to rotation in reverse direction over the entire operating range at pitch angle -10^0 and 10^0.

References

[1] A.S. Bahaj, L. Meyers, P.A.B. James, Urban energy generation: influence of micro-wind turbine output on electricity consumptions in buildings, Energy and Buildings 39 (2) (February 2007) 154–165.
[2] S. Mertens, Wind Energy in the Built Environment, Multiscience Publishing, 2006.
[3] W. Tong, W. Langreder, A.P. Schaffarczyk, S.G. Voutsinas, R.Z. Szasz, L. Fuchs, L.D. Willey, L. Staudt, P. Cooper, C. Lewis, T. Kanemoto, K. Kubo, D. Zheng, S. Bose, H. Matsumiya, B.F. Sorensen, J.W. Holmes, P. Brondsted, K. Branner, A.W. Hulskamp, H.E.N. Bersee, R. Hicks, B. Basu, J. van der Tempel, D. Diepeveen, N.F.B.J. Cerda Salzmann, de Vries, W.E.P. Milan, M. Wachter, S. Barth, J. Peinke, Y. Jiang, P. Pantazopoulou, M. Leahy, D. Connolly, N. Buckley, Wind Power Generation and Wind Turbine Design, WIT Press, Southampton, UK, May 28, 2010.
[4] M.H. Mohamed, Performance investigation of H-rotor darrieus turbine with new airfoil shapes, Energy 47 (1) (November, 2012) 522–530.
[5] I. Paraschivoiu, Wind turbine design: with emphasis on Darrieus concept, Polytechnic International Press, 2002.
[6] S. Ferreira, H. Bijl, G. van Bussel, G. van Kuik, "Simulating dynamic stall in a 2D VAWT: modeling strategy, verification and validation with particle image velocimetry data", the science of making torque from wind, J. Phys. Conf. Ser. 75 (2007).
[7] S. Wang, Z. Tao, L. Ma, D. Ingham, M. Pourkashanian, Numerical investigations on dynamic stall associated with low Reynolds number flows over airfoils, in: 2nd International Conference on Computer Engineering and Technology (ICCET), 16–18 April, 2010. Chengdu (China).
[8] V. Kumar, M. Paraschivoiu, I. Paraschivoiu, "Low Reynolds number vertical axis wind turbine for Mars", Wind Eng. 34 (4) (June 2010).
[9] M.R. Castelli, E. Benini, "Effect of blade inclination angle on a Darrieus wind turbine", Journal of Turbomach. 133 (October 2011).
[10] M.R. Castelli, G. Pavesi, E. Benini, L. Battisti, G. Ardizzon, Modeling strategy and numerical validation for a Darrieus vertical axis micro-wind turbine", in: Proceedings of the ASME 2010 International Mechanical Engineering Congress & Exposition, 12–18 November 2010, Vancouver, British Columbia, IMECE2010-39548.
[11] M.R. Castelli, E. Benini, Effect of blade thickness on Darrieus vertical-axis wind turbine performance, in: CSSim 2011, 2nd International Conference on Computer Modelling and Simulation, 5–7 September 2011, Brno (Czech Republic).
[12] M.H. Mohamed, G. Janiga, E. Pap, D. Thévenin, Optimal blade shape of a modified Savonius turbine using an obstacle shielding the returning blade, Energy Convers. Manage. 52 (1) (2011) 236–242.
[13] M.H. Mohamed, Impacts of solidity and hybrid system in small wind turbines performance, Energy 57 (2013) 495–504.
[14] M.H. Mohamed, Aero-acoustics noise evaluation of H-rotor darrieus wind turbines, Energy 65 (2014) 596–604.
[15] O. Guerri, A. Sakout, K. Bouhadef, Simulations of the fluid flow around a rotating vertical axis wind turbine, Wind Eng. 31 (2007) 149–163.
[16] W. Chen, C.Y. Zhou, Application of Numercal Simulation to Obtain the Optimization Pitch Angle for VAWT, IEEE, 2009, pp. 4244–4702.
[17] R. Howell, N. Qin, J. Edwards, N. Durrani, Wind tunnel and numerical study of a small vertical axis wind turbine, Renewable Energy 35 (2009) 412–422.
[18] M.C. Claessens, The Design and Testing of Airfoils for Application in Small Vertical Axis Wind Turbines, Delft University of Technology, 2006. MS thesis.
[19] P. Sabaeifard, H. Razzaghi, A. Forouzandeh, Determination of vertical Axis wind turbines optimal configuration through CFD simulations, in: International Conference on Future Environment and Energy, 2012. Singapore.
[20] F.L. Ponta, J.J. Seminara, A.D. Otero, On the aerodynamics of variable-geometry oval-trajectory Darrieus wind turbines, Renewable Energy 32 (1) (2007) 35–56.
[21] M.R. Castelli, A. Englaro, E. Benini, The Darrieus wind turbine: proposal for a new performance prediction model based on CFD, Energy 36 (6) (2011) 4919–4934.

Please cite this article in press as: M.H. Mohamed, et al., CFD analysis for H-rotor Darrieus turbine as a low speed wind energy converter, Engineering Science and Technology, an International Journal (2014), http://dx.doi.org/10.1016/j.jestch.2014.08.002